Infrared features of unquenched finite temperature lattice Landau gauge QCD

Sadataka Furui*
School of Science and Engineering, Teikyo University, 320-8551 Japan.

Hideo Nakajima†
Department of Information Science, Utsunomiya University, 321-8585 Japan.

(Dated: December 12, 2006)

The color diagonal and color antisymmetric ghost propagators of finite temperature $N_f = 2$ MILC $24^3 \times 12$ lattices are measured and compared with zero temperature unquenched $N_f = 2+1$ MILC$_c$ $20^3 \times 64$ and MILC$_f$ $28^3 \times 96$ lattices and zero temperature quenched 56^4 $\beta = 6.4, 6.45$ lattices. The expectation value of the color antisymmetric ghost propagator $\phi^c(q)$ is zero but its Binder cumulant, which is consistent with that of $N_c^2 - 1$ dimensional Gaussian distribution below T_c, becomes smaller above T_c. We study l^1 norm of $\phi^c(q)$ which could contain information on the ghost condensate parameter v. Although the color diagonal ghost propagator is temperature independent, the l^1 norm of the color antisymmetric ghost propagator is temperature dependent.

We also measure magnetic and electric gluon screening masses slightly above T_c. The running coupling at 0 momentum near T_c are almost constant but the magnetic gluon screening mass has temperature dependence. It implies strong non-perturbative effects in the magnetic screening mass of the gluon near T_c. The expectation values of the A^2 condensate and the ghost condensate in $T > T_c$ are consistent with 0.

PACS numbers: 12.38.Gc, 12.38.Aw, 11.10.Gh, 11.15.Ha, 11.15.Tk, 11.30.Rd

I. INTRODUCTION

As a condition of the color confinement in the infrared region, Kugo-Ojima criterion[1] and the Gribov-Zwanziger scenario[2, 3] are well-known. In these theories, infrared divergence of the ghost propagator is the essential ingredient of the emergence of the string-like inter-quark potential. Recently in finite temperature SU(3) lattice Coulomb gauge simulation, string-like structure was observed to remain above the deconfinement temperature T_c. Coulomb gauge is a non-covariant gauge and the momentum in the time direction is not affected by the gauge fixing. In finite temperature, the momentum in the time direction is interpreted as the Matsubara frequency with appropriate boundary conditions. The Landau gauge is a covariant gauge, and in the analysis of the quenched and unquenched lattice Landau gauge simulation[4, 5], we observed that the Kugo-Ojima parameters of the zero temperature unquenched configuration of the SU(3) MILC collaboration of $20^3 \times 64$ $\beta_{imp} = 6.76, 6.83$ (MILC$_c$), and $28^3 \times 96$ $\beta_{imp} = 7.09, 7.11$ (MILC$_f$) are consistent with 1 while the quenched configuration of 56^4 lattice remained about 0.8. The Binder cumulant of the color anti-symmetric ghost propagator of the zero temperature quenched SU(2) and unquenched SU(3) configurations of the MILC collaboration were consistent with those the N_c^2-1 dimensional Gaussian distribution, where N_c is the number of colors. The dynamical quark has the effect of quenching randomness of the system.

In this paper, we extend the analysis of the color anti-symmetric ghost propagator to the quenched SU(3) 56^4 lattices of $\beta = 6.4$ and 6.45[5] and the finite temperature unquenched SU(3) $24^3 \times 12$ configurations of the MILC collaboration[6]. The ghost propagator contributes in the off-shell quark gluon vertex via Ward-Slavnov-Taylor identity[7], and so we expect the screening masses of the gluons produced by the quark loops and ghost loops would be affected by the ghost propagator. We study the magnetic and the electric screening mass of the gluon of the MILC finite temperature $N_f = 2$ configurations of $\beta = 5.65, 5.725, 5.85$.

In the analysis of [8], the three configurations corresponds to the temperature $T = 143, 172.5$ and 185 MeV$_\rho$, respectively where subscript $_\rho$ means that the scale is fixed from the mass of the ρ meson $m_\rho = 770$MeV, and the temperature T_c that the cross over to the deconfinement occurs was assigned to be about 140MeV from the data of chiral susceptibility. Since the standard Wilson plaquette action was used in the production of the gauge configuration, the flavor symmetry was broken and the ratio of the ρ mass to pion mass is larger than the physical value[9]. Recent simulation with Asqtad action[10] suggests that $T_c \sim 170$MeV, consistent with the value of that of $N_f = 2$ improved Kogut-Susskind (KS) fermion $T_c \sim 173 \pm 8$MeV [11].

Since the continuum limit of the mass of the vector meson would not depend on the temperature near T_c[12], it would be natural to assign the bare lattice ρ mass by about 20% heavior and shift the temperature by the same amount. We leave a more accurate assignment of the temperature scale of the MILC$_{ft}$ to a future study and assign the $\beta = 5.65, 5.725$ and 5.85 data by $T/T_c =$

*Electronic address: furui@umb.teikyo-u.ac.jp; URL: http://albert.umb.teikyo-u.ac.jp/furui_lab/furuipbs.htm
†Electronic address: nakajima@is.utsunomiya-u.ac.jp

1.02, 1.23 and 1.32, respectively. We compare quenched and unquenched ghost propagator of zero temperature and finite temperature and investigate the role of quarks on the gluon field and its dependence on the temperature.

The organization of the paper is as follows. In the Sect.2, we show the results of the color diagonal ghost propagator of the quenched 56^4 and unquenched finite temperature MILC configurations. The corresponding color antisymmetric ghost propagators are shown in the Sect.3. The Kugo-Ojima parameters, the screening masses and the QCD running coupling of the finite temperature unquenched configurations are shown in the Sects.4, 5 and 6, respectively. Conclusions and a discussion are given in the Sect.7

II. THE COLOR DIAGONAL GHOST PROPAGATOR

The ghost propagator is defined by the Fourier transform(FT) of the expectation value of the inverse Faddeev-Popov(FP) operator $\mathcal{M} = -\partial_\mu \mathcal{D}_\mu$, where D_μ is the covariant derivative, as

$$\begin{aligned} FT[D_G^{ab}(x,y)] &= FT\langle \mathrm{tr}(\Lambda^{a\dagger}\{(\mathcal{M}[U])^{-1}\}_{xy}\Lambda^b)\rangle, \\ &= \delta^{ab} D_G(q^2). \end{aligned} \quad (1)$$

where U is the link variable obtained by the Landau gauge fixing. In all the simulation in this work we adopt the $\log U$ definition of the gauge field, and the SU(3) color matrix Λ is normalized as $\mathrm{tr}\Lambda^a\Lambda^b = \delta^{ab}$. Number of samples is about 10 each in the 56^4 lattices and about 100 each in the $24^3 \times 12$ lattices.

The color diagonal ghost propagator is defined as

$$\begin{aligned} &D_G(q) = \frac{1}{N_c^2-1}\frac{1}{V} \\ &\times \mathrm{tr}\left\langle \delta^{ab}(\langle \Lambda^a \cos \mathbf{q}\cdot\mathbf{x}|f_c^b(\mathbf{x})\rangle + \langle \Lambda^a \sin \mathbf{q}\cdot\mathbf{x}|f_s^b(\mathbf{x})\rangle)\right\rangle \\ &= G(q^2)/q^2 \end{aligned}$$

Here ${f_c}^b(\mathbf{x})$ and ${f_s}^b(\mathbf{x})$ are the solution of $\mathcal{M}f^b(\mathbf{x}) = \rho^b(\mathbf{x})$ with $\rho^b(\mathbf{x}) = \frac{1}{\sqrt{V}}\Lambda^b \cos \mathbf{q}\cdot\mathbf{x}$ and $\frac{1}{\sqrt{V}}\Lambda^b \sin \mathbf{q}\cdot\mathbf{x}$, respectively.

A. Quenched SU(3) 56^4 lattice

The color diagonal ghost propagators of 56^4 quenched SU(3) are shown in [5], but we show the data for a comparison with the color anti-symmetric ghost propagator in the next subsection. The FIG. 2 is the ghost dressing function, of the 56^4 $\beta = 6.45$ configurations produced@by the Monte-Carlo simulation and subsequently Landau gauge fixed.

The scale of the $\beta = 6.4$ and 6.45 configurations are fixed as in TABLE I. The ghost propagator is infrared divergent, but its singularity is weaker than q^{-4}.

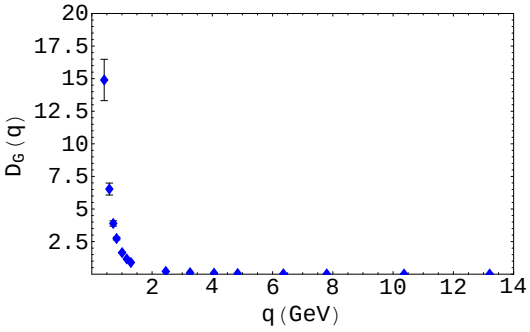

FIG. 1: The ghost propagator of quenched 56^4 configurations of $\beta = 6.45$(blue triangles).

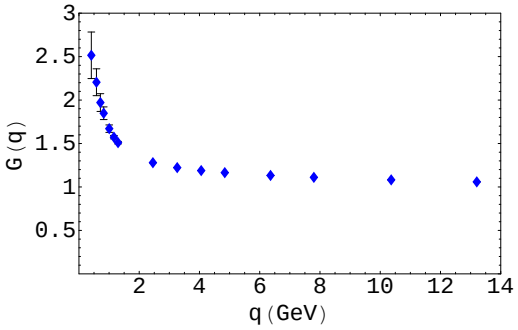

FIG. 2: The ghost dressing function of quenched 56^4 configurations of $\beta = 6.45$(blue triangles).

B. MILC finite temperature $24^3 \times 12$ lattice

The color diagonal ghost propagator and the ghost dressing function of MILC finite temperature configurations are shown in FIGs. 3 and 4, respectively. We observe that the three data of different temperatures scale

TABLE I: β_{imp}/β, the inverse lattice spacing $1/a$, lattice size and lattice length(fm) of configurations investigated in this paper. Subscripts c and f of MILC correspond to coarse lattice(a=0.12fm) and fine lattice(a=0.09fm). $\beta_{imp} = 5/3\times\beta$.

	β_{imp}/β	am_{ud}/am_s	N_f	$1/a$(GeV)	L_s	L_t	aL_s(fm)
quench	6.4		0	3.66	56	56	2.96
	6.45		0	3.87	56	56	2.94
MILC$_c$	6.83	0.040/0.050	2+1	1.64	20	64	2.41
	6.76	0.007/0.050	2+1	1.64	20	64	2.41
MILC$_f$	7.11	0.0124/0.031	2+1	2.19	28	96	2.52
	7.09	0.0062/0.031	2+1	2.19	28	96	2.52
MILC$_{ft}$	5.65	0.008	2	1.716	24	12	2.76
	5.725	0.008	2	1.914	24	12	2.47
	5.85	0.008	2	2.244	24	12	2.11

as shown in these figures.

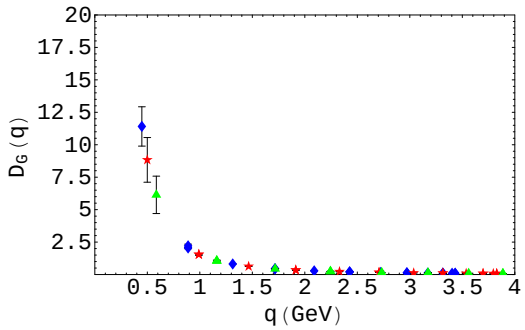

FIG. 3: The ghost propagator of MILC$_{ft}$ configurations of $T/T_c = 1.02$(blue diamonds), $T/T_c = 1.23$(red stars) and $T/T_c = 1.32$(green triangles).

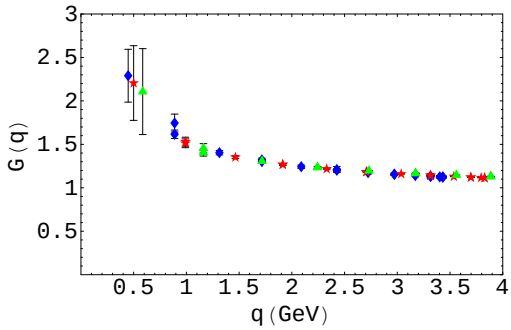

FIG. 4: The ghost dressing function of MILC$_{ft}$ configurations of $T/T_c = 1.02$(blue diamonds), $T/T_c = 1.23$(red stars) and $T/T_c = 1.32$(green triangles).

III. THE COLOR ANTISYMMETRIC GHOST PROPAGATOR

The color anti-symmetric ghost propagator is defined as

$$\phi^c(q) = \frac{1}{\mathcal{N}}\frac{1}{V} \times \mathrm{tr}\left\langle f^{abc}(\langle \Lambda^a \cos \mathbf{q}\cdot\mathbf{x}| f_s^b(\mathbf{x})\rangle - \langle \Lambda^a \sin \mathbf{q}\cdot\mathbf{x}| f_c^b(\mathbf{x})\rangle)\right\rangle$$

where the outer-most bracket means the ensemble average.

In a theory based on the Curci-Ferrari gauge and in its extension to the Landau gauge, a parameterization of the color anti-symmetric ghost propagator with use of the ghost condensate parameter v was proposed[13]. A simulation in the SU(2) lattice Landau gauge using a parametrization

$$\frac{1}{N_c^2-1}\sum_a |\phi^a(q)| = \frac{r/L^2 + v}{q^4 + v^2}$$

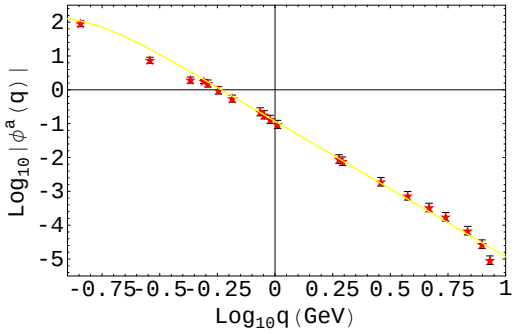

FIG. 5: $\log_{10}|\vec{\phi}(q)|$ as the function of $\log_{10} q$(GeV) of MILC$_f$ and the fit using $r = 134$ and $v = 0.026\mathrm{GeV}^2$.

is performed in [14] and that of the zero temperature MILC$_c$ and MILC$_f$ are performed in [15, 16].

Another quantity that characterizes the system is the Binder cumulant of the color antisymmetric ghost propagator defined as

$$U(q) = 1 - \frac{\langle \vec{\phi}(q)^4\rangle}{3\langle \vec{\phi}(q)^2\rangle^2}.$$

A simulation of SU(2) lattice Landau gauge obtained $U \sim 0.44$, almost independent of the momentum. This value is compatible with that of the three dimensional Gaussian distribution[15] and the analysis of SU(3) MILC$_c$ and MILC$_f$ showed that it is compatible with that of eight dimensional Gaussian distribution. We extend these analyses to large quenched lattices and the finite temperature configurations.

A. Quenched SU(3) 56^4 lattice

The absolute value of the color antisymmetric ghost propagator of@quenched@ 56^4 lattice is about 3 orders of magnitude smaller than that of the color diagonal ghost propagator. The Binder cumulant of the color antisymmetric ghost propagator of quenched configurations is noisy.

B. MILC zero temperature $28^3 \times 96$ lattice

The color antisymmetric ghost propagator of MILC$_f$ is shown in FIG. 5. Details of the fitting procedure are presented in [16]. The expectation value of v is small but the presence of BRST partner of A^2 condensate is suggested.

The Binder cumulant of the zero temperature MILC$_c$ lattice is reported in [15] and that of MILC$_f$ is reported in [16]. We observed that the mass function of $m_0 = 27.2$MeV quark propagator of $\beta_{imp} = 7.09$ with bare mass combination $m_0 = 27.2$MeV/68MeV shows an anomalous behavior in $q < 1$GeV region, and

that in the same region Binder cumulant $U(q)$ shows an anomalous behavior, although the mass function of $m_0 = 68$MeV does not show the anomaly. The non-QCD like behavior of staggered quarks calculated with large lattice spacing a and small bare mass m_0 is reported in [17]. Since no anomaly was observed in $\beta = 7.09$ $m_0 = 13.6$MeV/68MeV [16, 18], the effects of the relative size of the quark masses and the number of N_f are to be further investigated.

C. MILC finite temperature $24^3 \times 12$ lattice

The fluctuation of the color antisymmetric ghost propagator around 0 was almost Gaussian in the case of zero temperature unquenched configurations[15, 16]. The logarithm of the absolute value of the color antisymmetric ghost propagator of finite temperature unquenched configurations as a function of the logarithm of the momentum is shown in the FIG. 6. In contrast to the color diagonal ghost propagator, the absolute value of the color antisymmetric ghost propagator depends on the temperature. The temperature dependence of the scale of ϕ defined by r can be expressed as roughly $r \sim 5.49a^{-4.23}$, where a is the lattice spacing at each temperature in the unit of GeV.

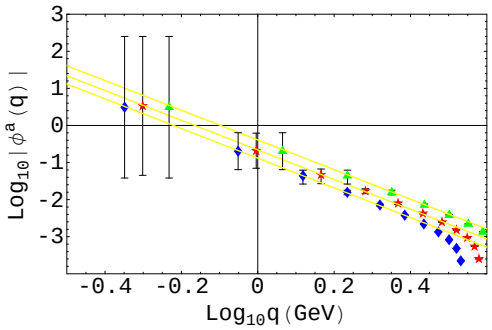

FIG. 6: $\log_{10}|\vec{\phi}(q)|$ as the function of $\log_{10}\vec{q}(GeV)$ of MILC$_{ft}$ of $T/T_c = 1.02$(blue diamonds), $T/T_c = 1.23$(red stars) and $T/T_c = 1.32$(green triangles).

The fitting parameters of the color anti-symmetric ghost propagator are given in TABLE II. The condensate parameter v of finite temperature is consistent with 0.

The Binder cumulant of ϕ is almost independent of the momentum except the lowest momentum point. We show a typical example of $T/T_c = 1.23$ in FIG. 7.

The temperature dependence of the average of $U(q)$ excluding the lowest momentum point is shown in FIG. 8. The deviation from the value of the Gaussian distribution indicated by the dashed line becomes large in high temperature.

TABLE II: The fitted parameters r, z and v of the color antisymmetric ghost propagator $|\phi(q)|$ of MILC$_c$, MILC$_f$ and MILC finite temperature. Two values of U of MILC$_f$ correspond to the average below $q = 1$GeV and the average above 1GeV, respectively.

β_{imp}/β	m_0(MeV)	r	z	v	U
6.76	11.5/82.2	37.5	3.90	0.012	0.53(5)
6.83	65.7/82.2	38.7	3.85	0.007	0.57(4)
7.09	13.6/68.0	134	3.83	0.026	0.57(4)/0.56(1)
7.11	27.2/68.0	112	3.81	0.028	0.58(2)/0.52(1)
5.65	12.3	54.4	4.01	0.0	0.580(13)
5.725	12.8	88.3	3.95	0.0	0.571(4)
5.85	15.0	165.9	3.93	0.0	0.558(2)

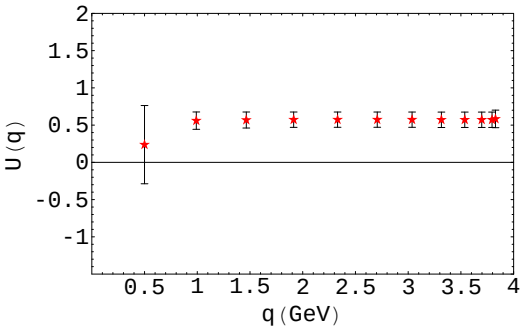

FIG. 7: The Binder cumulant of the color antisymmetric ghost propagator of MILC $N_f = 2$ configurations of $T/T_c = 1.23$(red stars).

IV. THE KUGO-OJIMA COLOR CONFINEMENT PARAMETER

The Kugo-Ojima parameter is defined by the two point function of the covariant derivative of the ghost and the commutator of the antighost and gauge field

$$\left(\delta_{\mu\nu} - \frac{q_\mu q_\nu}{q^2}\right) u^{ab}(q^2)$$
$$= \frac{1}{V}\sum_{x,y} e^{-ip(x-y)} \left\langle \mathrm{tr}\left(\Lambda^{a\dagger} D_\mu \frac{1}{-\partial D}[A_\nu, \Lambda^b]\right)_{xy}\right\rangle. \quad (2)$$

Kugo and Ojima[1] showed that $u(0) = -1$ is a condition of the color confinement. Zwanziger[3] defined the horizon function h that is related to the Kugo-Ojima parameter $c = -u(0)$ as follows.

$$\sum_{x,y} e^{-ip(x-y)} \left\langle \mathrm{tr}\left(\Lambda^{a\dagger} D_\mu \frac{1}{-\partial D}(-D_\nu)\Lambda^b\right)_{xy}\right\rangle$$

$$= G_{\mu\nu}(p)\delta^{ab} = \left(\frac{e}{d}\right)\frac{p_\mu p_\nu}{p^2}\delta^{ab} - \left(\delta_{\mu\nu} - \frac{p_\mu p_\nu}{p^2}\right) u^{ab},$$

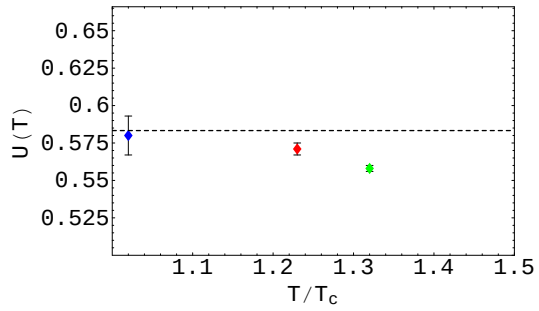

FIG. 8: Averages over momenta excluding the lowest momentum point of the Binder cumulants of MILC finite temperature configurations. $T/T_c = 1.02$(blue diamonds), $T/T_c = 1.23$(red stars) and $T/T_c = 1.32$(green triangles).

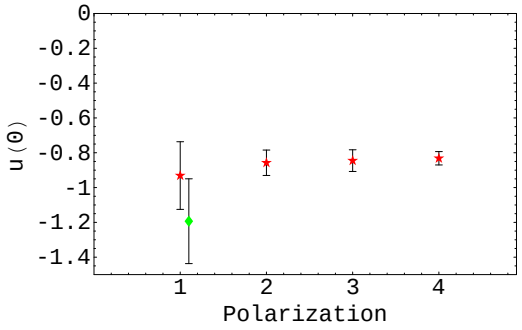

FIG. 9: Kugo-Ojima parameter $u(0)$ of quenched 56^4 configurations of $\beta = 6.45$(red stars). The data of an exceptional sample is indicated by the green diamond. Polarizations 1,2,3,4 correspond to x, y, z and t.

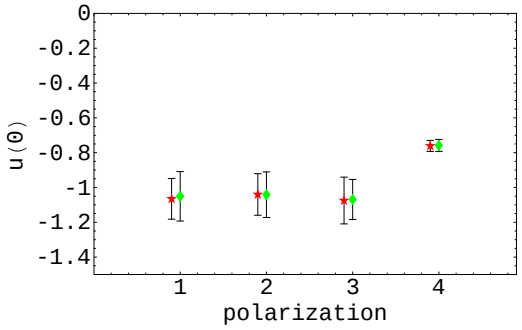

FIG. 10: Kugo-Ojima parameter $u(0)$ of MILC$_f$ $N_f = 2+1$ KS fermion unquenched configurations of $\beta_{imp} = 7.11$(green diamonds), $\beta_{imp} = 7.09$(red stars) .

where, with use of the covariant derivative $D_\mu(U)$

$$D_\mu(U_{x,\mu})\phi = S(U_{x,\mu})\partial_\mu\phi + [A_{x,\mu}, \bar{\phi}],$$

$\partial_\mu\phi = \phi(x+\mu) - \phi(x)$, $\bar{\phi} = \dfrac{\phi(x+\mu)+\phi(x)}{2}$ and $S(U_{x\mu}) = \dfrac{adjA_{x,\mu}/2}{\tanh(adjA_{x,\mu}/2)}$.

Using the definition

$$e = \left\langle \sum_{x,\mu} \mathrm{tr}(\Lambda^{a\dagger} S(U_{x,\mu})\Lambda^a) \right\rangle / \{(N_c^2-1)V\},$$

the horizon condition reads $\lim_{p\to 0} G_{\mu\mu}(p) - e = 0$, and the left hand side of the condition is $\left(\dfrac{e}{d}\right) + (d-1)c - e = (d-1)h$ where $h = c - \dfrac{e}{d}$ and dimension $d = 4$, and it follows that $h = 0 \rightarrow$ horizoncondition, and thus the horizon condition coincides with Kugo-Ojima criterion provided the covariant derivative approaches the naive continuum limit, i.e., $e/d = 1$.

A. Quenched SU(3) 56^4 lattice

The Kugo-Ojima confinement parameter of quenched configuration saturates at about 80% of the expected value $c = 1$. There appear exceptional samples with an average consistent with $c = 1$ within errors. The polarization dependence of the Kugo-Ojima parameter of $\beta = 6.45$ samples is shown in FIG. 9.

B. MILC finite temperature $N_f = 2$, $24^3 \times 12$ lattice

Kugo-Ojima parameter of zero temperature unquenched MILC$_c$ and MILC$_f$ configurations are consistent with the theory[15, 16, 19].

Kugo-Ojima parameter of unquenched configuration of the MILC$_{ft}$ depends on the temperature, as shown in the

TABLE III. The FIGs. 10 and 11 show the dependence on the polarization used in measuring the Kugo-Ojima parameter. The dependence on the polarization indicates that c becomes large when there is a long axis perpendicular to the polarization. It is because c appears after integration over the axes perpendicular to the polarization. The FIG. 11 shows the temperature dependence of the Kugo-Ojima parameter.

The quenched configurations and high temperature configurations, which have higher randomness show larger deviation from $u(0) = -1$. The origin of the randomness in the latter is due to thermal fluctuation and that of the former is due to the lack of fermions that quench randomness of the system.

V. THE FINITE TEMPERATURE GLUON PROPAGATOR

The one-loop off-shell contribution to the quark-gluon vertex, is related to the quark-quark-ghost-ghost amplitude via Ward-Slavnov-Taylor (WST) identity[7]. The screening mass of the gluon would be affected by the

	β_{imp}/β	c_x	c_t	c	e/d	h
quench	6.4			0.827(27)	0.954(1)	-0.12
	6.45			0.814(89)	0.954(1)	-0.14
MILC$_c$	6.76	1.04(11)	0.74(3)	0.97(16)	0.9325(1)	0.03(16)
	6.83	0.99(14)	0.75(3)	0.93(16)	0.9339(1)	-0.00(16)
MILC$_f$	7.09	1.06(13)	0.76(3)	0.99(17)	0.9409(1)	0.04(17)
	7.11	1.05(13)	0.76(3)	0.98(17)	0.9412(1)	0.04(17)
MILC$_{ft}$	5.65	0.72(13)	1.04(23)	0.80(21)	0.9400(7)	-0.14(21)
	5.725	0.68(15)	0.77(16)	0.70(15)	0.9430(2)	-0.24(15)
	5.85	0.63(19)	0.60(12)	0.62(17)	0.9465(2)	-0.33(17)

TABLE III: The Kugo-Ojima parameter of the quenched 56^4 lattice and that of the unquenched KS fermion (MILC$_c$,MILC$_f$,MILC$_{ft}$). The polarization along the spatial directions c_x and that along the time direction c_t and the average c, trace divided by the dimension e/d, horizon function deviation h are shown.

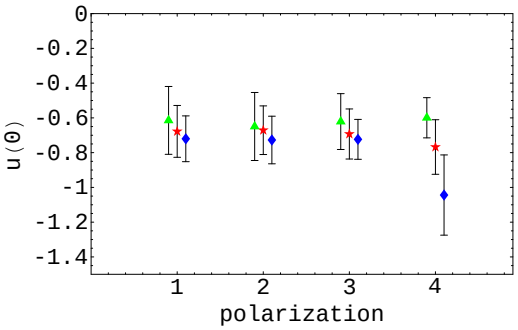

FIG. 11: Kugo-Ojima parameter $u(0)$ of MILC finite temperature configurations of $T/T_c = 1.02$(blue diamonds), $T/T_c = 1.23$(red stars) and $T/T_c = 1.32$(green triangles).

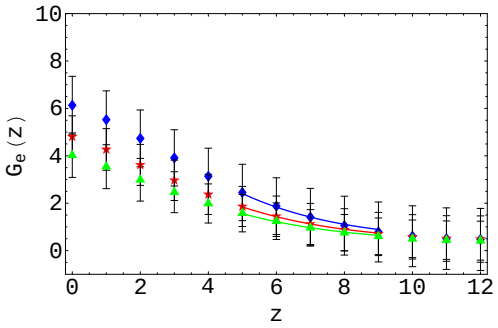

FIG. 12: Electric screening mass of MILC $N_f = 2$ KS fermion unquenched configuration of $T/T_c = 1.02$(blue diamonds), $T/T_c = 1.23$(red stars) and $T/T_c = 1.32$(green triangles).

ghost propagator. The correlation function of the gauge fields in the position space is defined as [20]

$$G_\mu(z) = \langle A_\mu(z) A_\mu(0) \rangle,$$

where $A_\mu(z) = \sum_{x_0,x_1,x_2} A_\mu(x_0, \vec{x})$.

The screening mass of the gluon is produced by the quark-, gluon- and ghost-loops. The electric screening mass m_e is defined by

$$G_e(z) = G_0(z) \sim exp[-m_e z/N_t T]$$

The magnetic screening mass m_m is defined by

$$G_m(z) = (G_1(z) + G_2(z))/2 \sim exp[-m_m z/N_t T]$$

We fit the correlator $G_e(z)$ and $G_m(z)$ by

$$G(z) = A \cosh[(m/N_t T)(z - N_x/2)].$$

The mass depends on the region of z used to fit the data and Karsch et al. proposed to fit data of z near $N_x/4$.[21] We fit the data from $z = 5$ to 9. When we fit the data from $z = 0$ to $z = 6$, the masses become smaller by about 30-40%. Since deviations from the cosh functional form become larger in this region, we adopt the fit from $z = 5$ to 9.

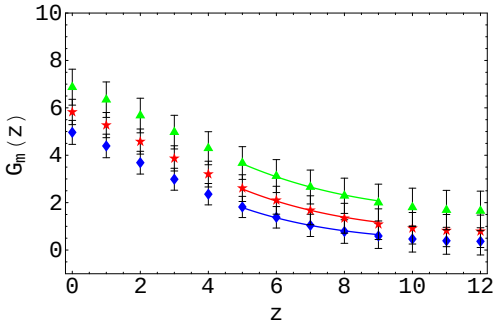

FIG. 13: Magnetic screening mass of MILC $N_f = 2$ KS fermion unquenched configurations of $T/T_c = 1.02$(blue diamonds), $T/T_c = 1.23$(red stars) and $T/T_c = 1.32$(green triangles).

The electric screening mass and the magnetic screening mass are close to those of SU(2) $m_e/T = 2.484(52)$ measured by [20]. The magnetic screening mass in the case of SU(2) is $m_m/T = 0.466(25)g^2(T)$ in the two-

TABLE IV: The electric and the magnetic screening mass

β	T/T_c	m_e/T	m_m/T
5.65	1.02	3.42(27)	3.48(48)
5.725	1.23	3.22(40)	2.90(20)
5.85	1.32	3.14(33)	2.31(22)

loop perturbative QCD (pQCD) calculation using $\Lambda_m = 0.262(18)T_c$.

In the quenched SU(3) Landau gauge QCD simulation, the critical temperature $T_c \sim 269 \pm 1$MeV[11], and the m_e/T and m_m/T from $T/T_c = 1.05$ to 5.61 were measured in [22]. Their data of $T/T_c = 1.32$ are consistent with ours within errors but near T_c our data are larger. We do not observe suppression of m_e/T near T_c. Whether the discrepancy is due to the presence of dynamical quarks is left for the future study.

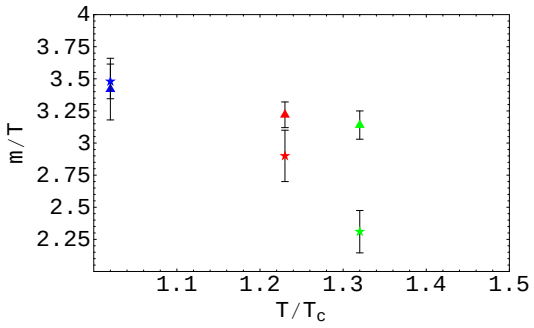

FIG. 14: The magnetic screening mass m_m/T (stars) and the electric screening mass m_e/T of MILC $N_f = 2$ KS fermion unquenched configurations (triangles) .

In high temperature, pQCD suggests that

$$\frac{m_e}{T} \propto g(T), \frac{m_m}{T} \propto g^2(T)$$

where $g^2(T)/4\pi$ is the running coupling at temperature T and 0 momentum. We measure the running coupling in the next section.

VI. THE FINITE TEMPERATURE QCD RUNNING COUPLING

We measured the QCD running coupling in the $\widetilde{MOM}$ scheme as the product of the gluon dressing function and the ghost dressing function squared, as a function of the momentum $\vec{q}$ along the spatial axes. We normalize the magnitude to the result of four-loop pQCD[19, 23, 24, 25] at the highest momentum point of $\beta = 5.725$. A Dyson-Schwinger equation (DSE) result of zero-temperature quenched configuration with the infrared exponent of the ghost propagator $\kappa = 0.5$ [26] is shown by the dashed line. Comparing with the result of $N_f = 2 + 1$ zero-temperature[19], the deviation from the pQCD is smaller. Although the presence of ghost condensate in zero-temperature is not clear, smallness of v and A^2 in finite temperatur is not unexpected.

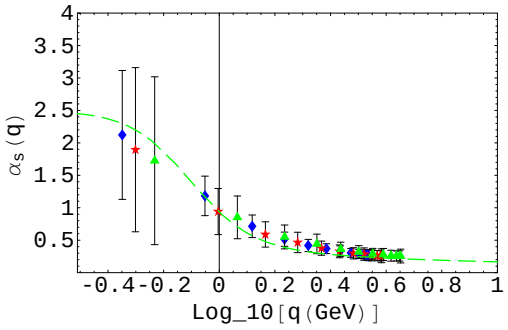

FIG. 15: The running coupling of the MILC finite temperature configurations of $\beta = 5.65$(blue diamonds), 5.725(red stars) and 5.85(green triangles) as the function of $\log \vec{q}$(GeV). Dashed line is the DSE result with $\kappa = 0.5$.

The running couplings of three temperatures near T_c as a function of the momentum $\vec{q}$ lies roughly on a single curve and there is not strong temperature dependence. The relatively large T dependence of the m_m/T suggests that the non-perturbative effects on the magnetic screening mass is important.

VII. DISCUSSION AND CONCLUSION

We measured the color diagonal and the color antisymmetric ghost propagator of quenched, unquenched zero temperature and unquenched finite temperature configurations. The quark has the effect of quenching randomness of the ghost propagator. The Binder cumulant of the quenched SU(3) color antisymmetric ghost propagator is noisy, but that of the unquenched SU(3) color antisymmetric ghost propagator is almost constant and independent of the momentum except the lowest momentum point. The color diagonal ghost propagators of finite temperatures scales above T_c, but the color antisymmetric ghost propagator do not scale. The scale of the color antisymmetric ghost propagator becomes larger as the temperature becomes higher.

We observed that the Binder cumulants of zero temperature unquenched SU(N) configurations are consistent with those $N^2 - 1$ dimensional Gaussian distribution. The Binder cumulants of finite temperature unquenched SU(3) configurations deviates from Gaussian distribution as the temperature rises, which may be interpreted as the effect of quenching randomness is reduced in high temperature. The anomaly of the KS fermion propagator and the anomaly of the momentum dependence of the Binder cumulant are correlated. It may indicate that the QCD-like region of $N_f = 2+1$ KS fermion system is more complicated than that of the $N_f = 2$ case given in [17].

We observed strong non-perturbative effects in the magnetic screening mass of the gluon near T_c. Since near T_c, systematic perturbative QCD calculation is impossible, it is important to formulate the lattice theory. In the quenched finite temperature Landau gauge DSE approach [27, 28] the infrared exponent κ and the running coupling in the MOM scheme were found to be essentially temperature independent below T_c.

We thank F. Karsch for a discussion on the scale assignment of the lattice data and A. Nakamura and T. Saito for the information on the quenched simulation of their group. This work is supported by the High Energy Accelerator Research Organization(KEK) supercomputer project No. 05-128 using Hitachi-SR8000 and the large scale simulation program No.5(FY2006) using SR11000. Numerical calculation of the ghost propagator was carried out by NEC-SX5 at the CMC of Osaka University and by NEC-SX8 at the Yukawa Institute Computer Facility. H.N. is supported by the MEXT grant in aid of scientific research in priority area No.13135210.

[1] T. Kugo and I. Ojima, Prog. Theor. Phys.(Kyoto) Suppl. **66**, 1 (1979).
[2] V.N. Gribov, Nucl. Phys. **B 139**1(1978).
[3] D. Zwanziger, Nucl. Phys. **B 364** ,127 (1991), idem B **412**, 657 (1994).
[4] S. Furui and H. Nakajima , Phys. Rev. D**69**,074505(2004); arXiv: hep-lat/0305010.
[5] S. Furui and H. Nakajima, Phys. Rev. D**70**,094504(2004); arXiv: hep-lat/0403021.
[6] C. Bernard et al., Phys. Rev. D**58**,014503(1998).
[7] A.I. Davydychev, P. Osland and L. Saks , Phys. Rev. D**63**,014022(2000).
[8] C. Bernard et al., Phys. Rev. D**54**,4585(1996).
[9] T. Blum, L. Kärkkäinen, D. Toussaint and S. Gottlieb, Phys. Rev. D**51**,5153(1995).
[10] C. Bernard et al., hep-lat/0611031.
[11] F. Karsch and E. Laermann; arXiv: hep-lat/0305025.
[12] F. Karsch, in *Selected topics in non perturbative QCD*, "Enrico Fermi School". p.51-71 (1995); arXiv: hep-lat/9512029.
[13] D. Dudal et al., J. High Energy Phys. 06, 003(2003).
[14] A.Cucchieri, T. Mendes and A. Mihara, Phys. Rev. D**72**,094505 (2005).
[15] S. Furui and H. Nakajima, Phys. Rev. D**73**,094506(2006); arXiv:hep-lat/0602027.
[16] S. Furui and H. Nakajima, Braz. J. Phys.,Proceedings of IRQCD in Rio, June 5-9 2006, in press; arXiv:hep-lat/0609024.
[17] A. Hasenfratz and R. Hoffmann, Phys. Rev. D**74**,014511(2006).
[18] S. Furui and H. Nakajima,Phys. Rev. D**73**,074503(2006); arXiv:hep-lat/0511045.
[19] S. Furui and H. Nakajima, Few Body Systems **40**,101 (2006) ; arXiv:hep-lat/0503029.
[20] U.M. Heller, F. Karsch and J. Rank , Phys. Lett. B**355**,511(1995); arXiv: hep-lat/9505016.
[21] U.M. Heller, F. Karsch and J. Rank , Phys. Rev. D**57**,1438(1998).
[22] A. Nakamura, T. Saito and S. Sakai, Phys. Rev. D**69**,014506(2004).
[23] Ph. Boucaud et al., JHEP **0201**,046 (2002) ; arXiv:hep-lat/0107278.
[24] K.G. Chetyrkin and A. Rétay ; arXiv:hep-ph/0007088; idem Nucl. Phys. **B583**,3(2000),arXiv:hep-ph/9910332.
[25] K.G. Chetyrkin, Nucl. Phys. **B710**,499(2005); arXiv:hep-ph/0405193 v3(2005).
[26] J.C. Bloch, Few Body Systems **33**,111 (2003).
[27] B. Grüter, R. Alkofer, A. Maas and J. Wambach, Eur. Phys. J. **C42**, 109(2005); arXiv:hep-ph/0408282.
[28] A. Maas, J. Wambach and R. Alkofer, Eur. Phys. J. **C42**, 93 (2005); arXiv:hep-ph/0504019.